Nucleic Acids Research, 2024, **52**, 10533–10542
https://doi.org/10.1093/nar/gkae695
Advance access publication date: 20 August 2024
Nucleic Acid Enzymes

Chemical synthesis of 2″OMeNAD$^+$ and its deployment as an RNA 2′-phosphotransferase (Tpt1) 'poison' that traps the enzyme on its abortive RNA-2′-PO$_4$-(ADP-2″OMe-ribose) reaction intermediate

Jakob Arnold[1,†], Shreya Ghosh[2,†], Renata Kasprzyk[1,†], Marcel Brakonier[1,†], Markus Hanna[1], Andreas Marx[1,*] and Stewart Shuman[2,*]

[1]Department of Chemistry, University of Konstanz, 78457 Konstanz, Germany
[2]Molecular Biology Program, Memorial Sloan Kettering Cancer Center, New York, NY 10065, USA

[*]To whom correspondence should be addressed. Email: shumans@mskcc.org
Correspondence may also be addressed to Andreas Marx. Email: andreas.marx@uni-konstanz.de
[†]The first four authors should be regarded as Joint First Authors.

Abstract

RNA 2′-phosphotransferase Tpt1 catalyzes the removal of an internal RNA 2′-PO$_4$ via a two-step mechanism in which: (i) the 2′-PO$_4$ attacks NAD$^+$ C1″ to form an RNA-2′-phospho-(ADP-ribose) intermediate and nicotinamide; and (ii) transesterification of the ADP-ribose O2″ to the RNA 2′-phosphodiester yields 2′-OH RNA and ADP-ribose-1″,2″-cyclic phosphate. Although Tpt1 enzymes are prevalent in bacteria, archaea, and eukarya, Tpt1 is uniquely essential in fungi and plants, where it erases the 2′-PO$_4$ mark installed by tRNA ligases during tRNA splicing. To identify a Tpt1 'poison' that arrests the reaction after step 1, we developed a chemical synthesis of 2″OMeNAD$^+$, an analog that cannot, in principle, support step 2 transesterification. We report that 2″OMeNAD$^+$ is an effective step 1 substrate for *Runella slithyformis* Tpt1 (RslTpt1) in a reaction that generates the normally undetectable RNA-2′-phospho-(ADP-ribose) intermediate in amounts stoichiometric to Tpt1. EMSA assays demonstrate that RslTpt1 remains trapped in a stable complex with the abortive RNA-2′-phospho-(ADP-2″OMe-ribose) intermediate. Although 2″OMeNAD$^+$ establishes the feasibility of poisoning and trapping a Tpt1 enzyme, its application is limited insofar as Tpt1 enzymes from fungal pathogens are unable to utilize this analog for step 1 catalysis. Analogs with smaller 2″-substitutions may prove advantageous in targeting the fungal enzymes.

Graphical abstract

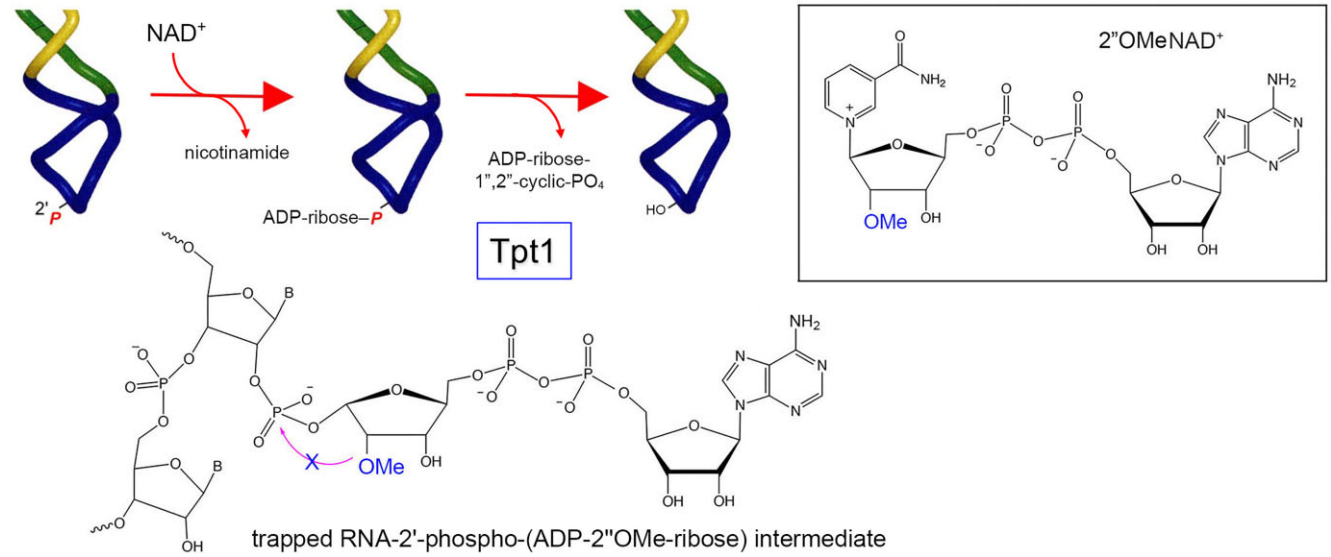

Received: June 17, 2024. **Revised:** July 24, 2024. **Editorial Decision:** July 25, 2024. **Accepted:** July 31, 2024

Introduction

ADP-ribosyl transferases are enzymes that catalyze nucleophilic attack on the C1″ atom of NAD+ with displacement of nicotinamide. If the nucleophile is water, ADP-ribose is the product. Diverse clades of ADP-ribosyl transferases, with distinct nucleophile substrate specificities, catalyze addition of ADP-ribose to proteins, nucleic acids, and metabolites, thereby imparting new properties and/or functions to the ADP-ribosylated products (1). Alternatively, ADP-ribosylation of a substrate nucleophile serves to activate that substrate for a second enzymatic step of nucleophilic attack by the vicinal O2″ on the ADP-ribosylated intermediate (as in Figure 1A). Two well-studied examples of the latter scenario are the sirtuin enzymes that catalyze lysine deacylation and the Tpt1 enzymes that catalyze the removal of internal RNA 2′-PO_4 groups. The sirtuin mechanism entails attack of the lysine acyl oxygen on NAD+ C1″ to form an acyl-lysine–ADPr alkylimidate intermediate and release nicotinamide, followed by attack of the ribose O2″ on the acyl carbon to release the deacylated lysine and form 2″O-acyl-ADP-ribose (2). There is considerable interest in the discovery of small molecule effectors that either inhibit or enhance the activity of sirtuin enzymes (3).

Tpt1 (tRNA 2′-phosphotransferase) is an essential enzyme in the fungal and plant tRNA splicing pathways that removes the 2′-PO_4 at the splice junction generated by fungal and plant tRNA ligases (4) (Figure 1A). Tpt1 orthologs are also widely prevalent in bacteria, metazoa and archaea, despite the absence in these taxa of fungal-type RNA ligases that form a 2′-PO_4 RNA (5–8). The Suzuki lab identified 2′-phosphouridine as a stable modification in the variable loop of tRNAs from several thermophilic archaea and proceeded to discover Ark1 as the archaeal RNA 2′-OH kinase that installs the internal tRNA 2′-PO_4 (9). Whereas Tpt1 can remove the 2′-PO_4 installed by Ark1, this activity is not essential for the archaeon, insofar as the Ark1 kinase is dispensable for viability (9). The endogenous substrates for Tpt1 in bacterial and metazoa are unknown and available evidence indicates that Tpt1 is nonessential in *E. coli* and mammals, where absence of Tpt1 elicits no apparent phenotype (5,10).

Tpt1 operates via a two-step chemical mechanism in which: (i) the internal RNA 2′-PO_4 attacks the C1″ atom of NAD+ to form an RNA-2′-phospho-(ADP-ribose) intermediate and expel nicotinamide and (ii) transesterification of the ADP-ribose O2″ to the 2′-phosphodiester yields 2′-OH RNA and ADP-ribose-1″,2″-cyclic phosphate products (7,11–15) (Figure 1A). There is no involvement of a divalent cation cofactor in the Tpt1 reaction (7). The kinetic mechanism, substrate specificity, and essential active site constituents of Tpt1 have been elucidated via studies of Tpt1 from the bacterium *Runella slithyformis* (7,8,15–17). Mechanistically informative crystal structures of Tpt1 from thermophilic bacteria and archaea have captured the enzyme at various stages along the reaction pathway, e.g. bound to NAD+ substrate, 2′,5′-ADP or NADP+ substrates (mimetics of a 2′-PO_4 RNA substrate), ADP-ribose-PO_4 product, and 2′-OH RNA product (15,18). Tpt1 consists of an N-terminal RNA lobe and a C-terminal NAD+ lobe connected via a protease-sensitive linker peptide (6,15). The available structures highlight how flipping of the 2′-PO_4 nucleobase into a Tpt1 surface crevasse and atomic contacts to the vicinal 3′-PO_4 and 2′-PO_4 groups ensure recognition of the splice junction. Tpt1 makes an extensive array of amino acid side-chain and main-chain contacts to the adenosine, diphosphate, and nicotinamide moieties of NAD+ that position the nicotinamide riboside adjacent to the 2′-PO_4 in preparation for step 1 chemistry at C1″. A network of essential enzymic contacts to the transferred 2′-PO_4 and the product RNA is imputed to stabilize the transition state of the step 2 transesterification reaction and promote expulsion of the 2′-OH leaving group.

Two key states along the Tpt1 pathway have not yet been amenable to structure determination: a Michaelis complex with NAD+ and a 2′-PO_4 RNA; and Tpt1 bound to an RNA-2′-phospho-(ADP-ribose) intermediate. The challenge is how to preclude step 1 chemistry (for the Michaelis complex) or step 2 chemistry (for the intermediate complex) without unduly altering the enzyme or the reactants so that one winds up in an off-pathway state. This challenge has been addressed for other ADP-ribosyltransferases via creative synthesis of minimally substituted NAD+ analogues that cannot support reaction chemistry. For example, carba-NAD+ has a methylene group in lieu of the NMN ribose O4″ and will not permit nicotinamide displacement (19,20). Arresting the subsequent step by a 2″-OH nucleophile should, in principle, be achievable by replacing the ribose 2″-OH with a 2″-OMe or a 2″-F substituent. In an approximation of this approach, a 2″-F substituted arabino-NAD+ analogue has been synthesized and investigated as an inhibitor of NAD+ glycohydrolase (21–23).

We reported previously that *Runella slithyformis* Tpt1 (RslTpt1), when reacted under conditions of enzyme excess with a 6-mer 2′-PO_4-branched RNA oligonucleotide substrate in the presence of 50 μM ara-2″F-NAD+ (which is commercially available), converted nearly all of the input RNA into an RNA-2′-phospho-(ADP-fluoroarabinose) dead-end product of step 1 of the Tpt1 pathway (17). Although the yield of 2′-phospho-(ADP-fluoroarabinose) 6-mer RNA was high for RslTpt1, the apparent step 1 rate constant with ara-2″F-NAD+ (0.077 min^{-1}) was at least two orders of magnitude slower than the step 1 rate constant observed with NAD+ (17,7). Structure modeling of ara-2″F-NAD+ in the Tpt1 active site suggested that the 'up' configuration of the ara-2″F moiety versus the 'down' conformation of the ribose-2″OH engenders a steric clash with an essential arginine side chain (17). Although this work established the feasibility of 'poisoning' the Tpt1 reaction via chemical modification of the NAD+ substrate, the arabinosyl analog is not a promising means to interdict Tpt1 function.

In the present study, we present a method for chemical synthesis of 2″OMeNAD+, an NAD+ analogue in which the ribose 2″-OH is replaced by a 2″-OMe group that should not serve as a nucleophile for step 2 transesterification in the Tpt1 pathway (Figure 1B). We find that 2″OMeNAD+ is an effective substrate for step 1 catalysis by RslTpt1 that leads to formation of an RNA-2′-phospho-(ADP-2″OMe-ribose) dead-end product at 1:1 stoichiometry to input enzyme, whereby RslTpt1 remains stably trapped in a complex with the dead-end product. Thus, 2″OMeNAD+ has two properties that recommend further development of 2′-substituted nicotinamide riboside derivatives as Tpt1 poisons: (i) it durably blocks step 2 transesterification, thereby turning a 'small' problem at the tRNA splice junction (the 2′-PO_4) in to a much bigger and bulkier lesion, a 2′-phospho-(ADP-2″OMe-ribose); and (ii) it sequesters Tpt1 on the lesion-containing RNA.

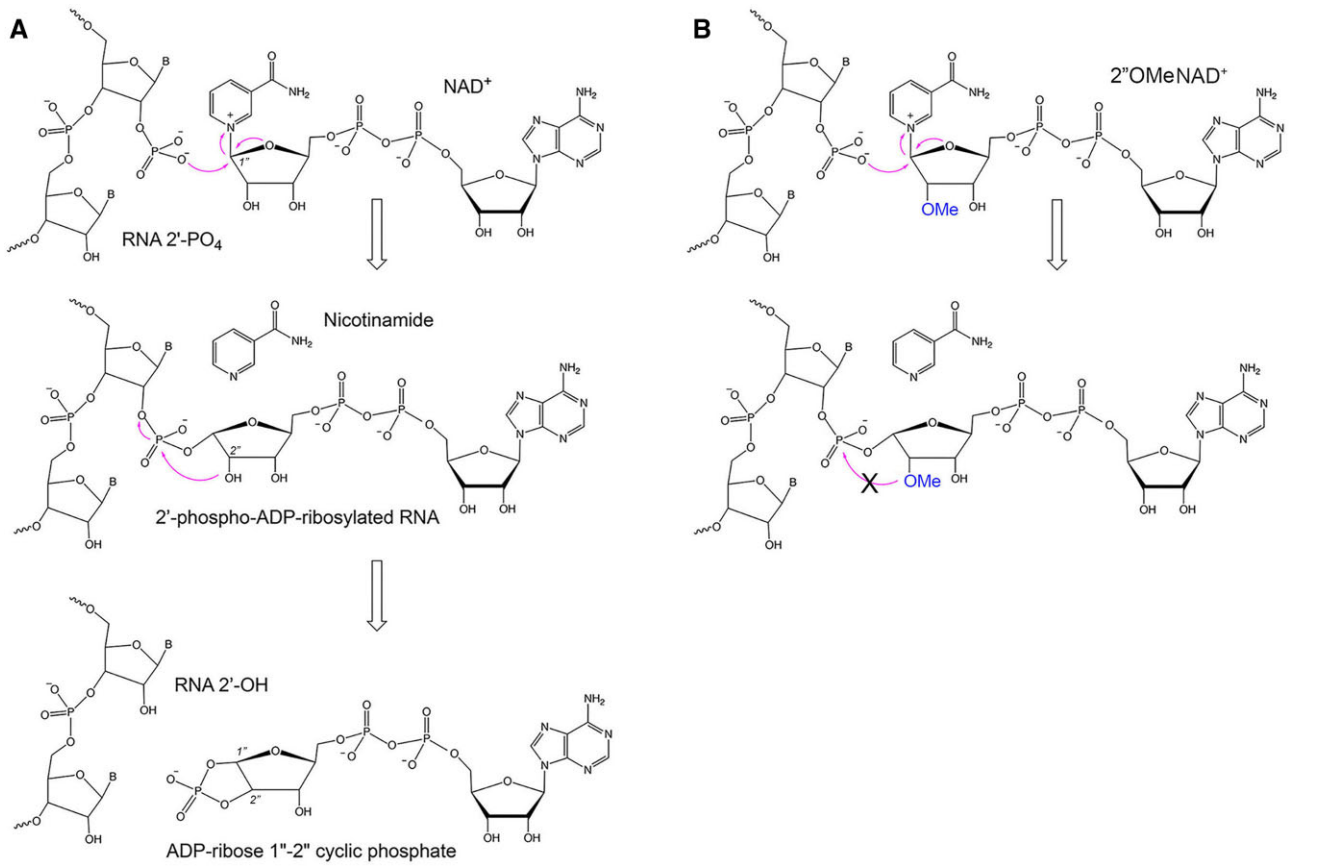

Figure 1. Tpt1 mechanism. (**A**) The Tpt1 reaction pathway comprises the two chemical steps shown in which: (1) an RNA 2′-PO_4 oxygen attacks the C1″ atom of NAD^+ to expel nicotinamide and form a 2′-phospho-ADP-ribosylated RNA intermediate and (2) transesterification of the ADP-ribose 2″-OH to the RNA 2′-PO_4 displaces the RNA 2′-OH and generates ADP-ribose-1″,2″-cyclic phosphate. (**B**) 2″OMeNAD^+ is an NAD^+ analogue in which the ribose 2″-OH is replaced by a 2″-OMe group that should not serve as a nucleophile for step 2 transesterification.

Materials and methods

General methods for chemical synthesis and product analysis are described in Supplementary Information.

1,2-Dimethoxy-3,5-*O,O*-((tetraisopropyl)disiloxanediyl)-β-D-ribofuranose (2)

Compound **1** (Figure 2A, 7.2 g, 17.8 mmol, 1 eq.), synthesized as described (29), was dissolved in dimethylformamide (DMF, 62 ml). Iodomethane (32 ml, 514 mmol, 29 eq.) and Ag_2O (12.1 g, 52.1 mmol, 3 eq.) were added and the reaction mixture was heated under reflux for 16 h. After cooling to room temperature, the suspension was filtered using Celite® and the filter was washed with dichloromethane (DCM, 40 ml). The filtrate was then washed with saturated $Na_2S_2O_3$ solution (2 × 60 ml). The phases were separated, the organic phase was dried over Na_2SO_4 and the solvent was removed under reduced pressure. The crude product was purified via flash column chromatography (40:1–10:1 hexanes/ethyl acetate, v/v) and compound **2** (Figure 2A) was obtained (6.3 g, 14.9 mmol, 84%). ^{1}H NMR (400 MHz, $CDCl_3$) δ 4.75 (s, 1H, H_1), 4.48 (dd, J = 7.8, 4.3 Hz, 1H, H_3), 4.04–3.94 (m, 2H, H_4, H_5), 3.92–3.82 (m, 1H, $H_{5'}$), 3.59 (d, J = 4.3 Hz, 1H, H_2), 3.57 (s, 3H, C_2-OMe), 3.32 (s, 3H, C_1-OMe), 1.14–0.94 (m, 28H, H_{iPr}).

3,5-Diacetoxy-1,2-dimethoxy-β-D-ribofuranose (3)

Compound **2** (4.5 g, 10.7 mmol, 1 eq.) was dissolved in dry tetrahydrofuran (THF, 20 ml). After the slow addition of tetrabutylammonium fluoride (TBAF) in THF (1 M, 4 ml), the reaction was stirred for 17 h at room temperature. After full conversion of the starting material, verified by thin layer chromatography (TLC), the reaction was quenched with methanol (10 ml). After removal of the solvents 1,2-dimethoxy-β-D-ribofuranose was used in the subsequent synthesis without further purification. The crude product was dissolved in pyridine (150 ml) and acetic anhydride (3 ml) was added dropwise at room temperature. The reaction was stirred for 19 h until TLC indicated complete conversion. The reaction was quenched by the addition of water (100 ml) and the aqueous phase was extracted with dichloromethane (3 × 150 ml). The combined organic phases were dried over Na_2SO_4, the solvent was removed under reduced pressure and the crude product was azeotroped with toluene (3 × 60 ml). After purification via flash column chromatography (3:1 hexanes/ethyl acetate, v/v), compound **3** (Figure 2A) was obtained (2.5 g, 9.6 mmol, 90% over two steps) as a yellow oil. ^{1}H NMR (400 MHz, $CDCl_3$) δ 5.09 (dd, J = 6.2, 4.8 Hz, 1H, H_3), 4.90 (d, J = 1.3 Hz, 1H, H_1), 4.37–4.26 (m, 2H, H_4, H_5), 4.13–4.05 (dd, J = 12.8, 7.0 Hz, 1H, $H_{5'}$), 3.87 (dd, J = 5.0, 1.3 Hz, 1H, H_2), 3.42 (s, 3H, C_2-OMe), 3.38 (s, 3H, C_1-OMe), 2.12 (s, 3H, OAc), 2.09 (s, 3H, OAc).

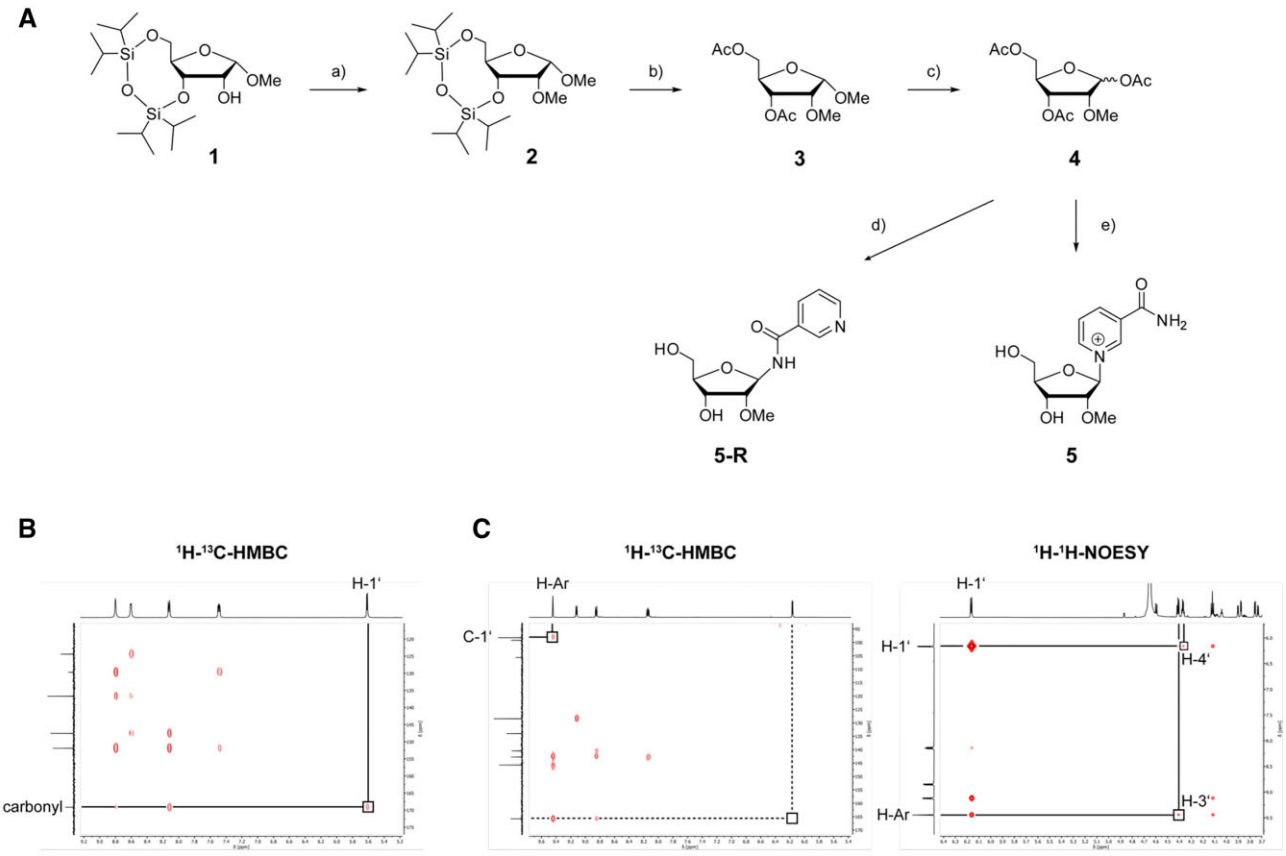

Figure 2. Synthesis of 2′OMe-nicotinamide riboside (compound **5**) using TMS-OTf mediated glycosylation. (**A**) (a) Iodomethane, Ag_2O, dimethylformamide, 80°C, 18 h, 84%. (b) tetrabutylammonium fluoride, tetrahydrofurane, r.t., 17 h; then acetic anhydride, pyridine, r.t., 19 h, 90% over two steps. (c) acetic acid, acetic anhydride, H_2SO_4, 10°C, 16 h, 71%. (d) nicotinamide, compound **4**, acetonitrile, then TMS-triflate, r.t., 4 h. (e) nicotinamide, TMS-triflate, acetonitrile, r.t. 30 min, then compound **4**, r.t., 4 h; then NH_3 in methanol, r.t., 18 h, 28% over two steps; (**B**) 1H-^{13}C-HMBC NMR spectrum of compound **5-R**, with highlighted cross signal between 1′-*H* and *C*-carbonyl. (**C**) 1H-^{13}C-HMBC NMR spectrum of compound **5** showing the absence of the carbonyl-correlation and instead a cross signal between 1′-*H* and *C*-2 and 1H-1H NOESY spectrum of compound **5** with highlighted nuclear overhauser effects (NOEs) between 1′-*H* and 4′-*H* and 3′-*H* and aromatic protons.

1,3,5-Triacetoxy-2-methoxy-β-D-ribofuranose (4)

Compound **3** (2.5 g, 9.6 mmol, 1 eq.) was dissolved in acetic acid (32 ml) and acetic anhydride (6.4 ml). After cooling to 10°C, H_2SO_4 (1.8 ml) was added dropwise, and the reaction mixture was stirred at room temperature for 16 h. The reaction mixture was poured on ice and the aqueous phase was extracted with dichloromethane (3 × 150 ml). The combined organic phases were washed with saturated $NaHCO_3$ solution (2 × 100 ml) and dried over Na_2SO_4. After removal of the solvents, the crude product was purified via flash column chromatography (1–5% methanol in dichloromethane, v/v) yielding compound **4** (Figure 2A, 1.1 g, 6.8 mmol, 71%) as a yellow oil. ^{1}H NMR (500 MHz, $CDCl_3$) δ 6.17 (d, J = 1 Hz, 1H, H_1), 5.04 (dd, J = 7.3, 4.9 Hz, 1H, H_3), 4.38 (ddd, J = 7.3, 5.5, 3.6 Hz, 1H, H_4), 4.32 (dd, J = 12.0, 3.6 Hz, 1H, H_5), 4.15–4.07 (m, 1H, $H_{5'}$), 3.99 (dd, J = 4.9, 1.0 Hz, 1H, H_2), 3.45 (s, 3H, C_2-OMe), 2.14 (s, 3H, OAc), 2.11–2.07 (2x s, 6H, 2x OAc).

1-(2′-Methoxy-β-D-ribofuranosyl)nicotinamide (5)

Nicotinamide (43 mg, 0.35 mmol, 1.03 eq.) was dissolved in acetonitrile (3 ml) and trimethylsilyl-trifluoromethanesulfonate (TMS-triflate, 0.5 ml, 2.76 mmol, 8 eq.) was added dropwise at 0°C. After stirring for 30 min, compound **4** (100 mg, 0.34 mmol, 1 eq. dissolved in 5 ml acetonitrile), was added and the mixture was stirred for 4 h at room temperature. After addition of methanol (5 ml) and removal of the solvents under reduced pressure, ammonia in methanol (7 N) was added and the mixture was stirred for 16 h at room temperature. The solvent was removed under reduced pressure and crude product was purified via preparative RP-HPLC using ammonium acetate buffer (50 mM) and acetonitrile as the mobile phase to give compound **5** (Figure 2A) as a white solid (26 mg, 0.10 mmol, 28% over two steps). ^{1}H NMR (500 MHz, D_2O) δ 9.54 (s, 1H, H_{2N}), 9.22 (d, J = 6.3 Hz, 1H, H_{6N}), 8.95 (dt, J = 8.1, 1.5 Hz, 1H, H_{4N}), 8.24 (dd, J = 8.1, 6.3 Hz, 1H, H_{5N}), 6.26 (d, J = 4.6 Hz, 1H, $H_{1'}$), 4.50 (t, J = 4.2 Hz, 1H, $H_{3'}$), 4.46 (m, 1H, $H_{4'}$), 4.21 (t, J = 4.8 Hz, 1H, $H_{2'}$), 3.98 (dd, J = 12.8, 2.8 Hz, 1H, $H_{5'}$), 3.84 (dd, J = 12.8, 3.5 Hz, 1H, $H_{5''}$), 3.49 (s, 3H, C_2'-OMe). ^{13}C NMR (126 Hz, D_2O) δ 165.78 (C_{Carb}), 145.75 (C_{4N}), 142.73 (C_{6N}), 140.44 (C_{2N}), 134.03 (C_{3N}), 128.47 (C_{5N}), 98.21 ($C_{1'}$), 88.73 ($C_{4'}$), 85.98 ($C_{2'}$), 68.51 ($C_{3'}$), 60.25 ($_{C5'}$), 58.45 ($C_{2'}$-OMe).

1-(2′-Methoxy-β-D-ribofuranosyl)nicotinamide-5′-O-monophosphate triethylammonium salt (6)

Compound **5** (20.8 mg, 78.1 µmol, 1 eq.) was dissolved in trimethylphosphate (TMP, 0.2 ml) and cooled to 0°C. After-

wards $POCl_3$ (27.4 µl, 296 µmol, 3.8 eq.) was added dropwise and the reaction mixture was stirred for 4 h at 0°C. After reaction termination upon addition of Milli-Q water (8 ml), the pH was adjusted to 7 with 0.1 M NaOH. The reaction mixture was then washed with ethyl acetate (3 × 10 ml) and the aqueous phase was purified by preparative RP-HPLC using a linear gradient of acetonitrile in triethylammonium acetate buffer (50 mM, pH 6). The collected eluate was repeatedly lyophilized to yield compound **6** (Figure 3) as a light yellow solid (17.6 mg, 39.4 µmol, 50%). ^{1}H NMR (500 MHz, D_2O) δ 9.47 (s, 1H, H_{2N}), 9.28 (dt, J = 6.4, 1.5 Hz, 1H, H_{6N}), 9.00 (dt, J = 8.0, 1.5 Hz, 1H, H_{4N}), 8.31 (dd, J = 8.0, 6.4 Hz, 1H, H_{5N}), 6.28 (d, J = 5.7 Hz, 1H, $H_{1'}$), 4.69–4.68 (m, 2H, $H_{3',4'}$), 4.36 (dd, J = 5.7, 4.3 Hz, 1H, $H_{2'}$), 4.30 (ddd, J = 12.1, 4.9, 2.1 Hz, 1H, $H_{5'}$), 4.14 (ddd, J = 12.1, 4.9, 2.1 Hz, 1H, $H_{5'}$), 3.53 (s, 3H, $C_{2'}$-OMe). ^{13}C NMR (126 MHz, D_2O) δ 165.92 ($C_{carb.}$), 146.17 (C_{4N}), 142.70 (C_{6N}), 139.89 (C_{2N}), 134.05 (C_{3N}), 128.62 (C_{5N}), 98.53 ($C_{1'}$), 88.56 ($C_{4'}$), 86.10 ($C_{2'}$), 69.38 ($C_{3'}$), 64.09 ($C_{5'}$), 58.36 ($C_{2'}$-OMe). ^{31}P NMR (202 MHz, D_2O) δ 0.75 (1P, s). HRMS (+)ESI m/z found: 349.0778, calc. for $C_{12}H_{18}N_2O_8P^+$: 349.0795.

1-(2′-Methoxy-β-D-ribofuranosyl)nicotinamide adenine dinucleotide (7)

Triethylammonium salt of compound **6** (14.2 mg, 31.8 µmol, 1 eq.) was combined with the sodium salt of adenosine-5′-monophosphate (AMP) *P*-imidazolide (26.7 mg, 63.6 µmol, 2 eq.; synthesized as described in (24) and $MgCl_2$ (30.2 mg, 318 µmol, 10 eq.) in formamide (1 ml). The reaction was conducted at room temperature for 24 h and terminated by adding water (7 ml). 2″OMe-NAD$^+$ was purified by preparative RP-HPLC using the same system and column as for compound **6**. For separation, a linear gradient of acetonitrile in 0.1% formic acid was applied. The collected eluate was repeatedly lyophilized to yield compound **7** (Figure 3, 2″OMe-NAD$^+$) as a white solid (10.6 mg, 15.4 µmol, 48%). ^{1}H NMR (500 MHz, D_2O) δ 9.42 (s, 1H, H_{2N}), 9.27 (dt, J = 6.2, 1.5 Hz, 1H, H_{6N}), 8.96 (dt, J = 8.2, 1.5 Hz, 1H, H_{4N}), 8.40 (s, 1H, H_{2A}), 8.31 (s, 1H, H_{8A}), 8.31 (dd, J = 8.2, 6.2 Hz, 1H, H_{5N}), 6.24 (d, J = 5.7 Hz, 1H, $H_{1'N}$), 6.16 (d, J = 5.5 Hz, 1H, $H_{1'A}$), 4.77–4.76 (m, 1H, $H_{2'A}$), 4.70 (dd, J = 4.8, 2.5 Hz, 1H, $H_{3'N}$), 4.65 (t, J = 2.5 Hz, 1H, $H_{4'N}$), 4.54 (dd, J = 5.1, 3.9 Hz, 1H, $H_{3'A}$), 4.43–4.41 (m, 1H, $H_{4'A}$), 4.41–4.38 (m, 1H, $H_{5'N}$), 4.36 (dd, J = 5.7, 4.8 Hz, 1H, $H_{2'N}$), 4.30–4.21 (m, 3H, $H_{5''N, 5'A, 5''A)}$, 3.52 (s, 3H, $C_{2'N}$-OMe). ^{13}C NMR (126 Hz, D_2O) δ 165.67 ($C_{carb.}$), 150.87 (C), 148.54 (C), 146.18 (C_{4N}), 146.12 (C_{8A}), 142.72 (C_{6N}), 142.07 (C_{2A}), 139.96 (C_{2N}), 133.98 (C_{3N}), 128.73 (C_{5N}), 98.45 ($C_{1'N}$), 88.10 ($C_{4'N}$), 87.77 ($C_{1'A}$), 85.88 ($C_{2'N}$), 84.15 ($C_{4'A}$), 74.57 ($C_{2'A}$), 70.34 ($C_{3'A}$), 69.10 ($C_{3'N}$), 65.20 ($C_{5'A}$), 64.97 ($C_{5'N}$), 58.35 ($C_{2'N}$-OMe). ^{31}P NMR (202 MHz, D_2O) δ −10.68 (1P, d, J = 20.9 Hz, P_a), -11.05 (1P, d, J = 20.9 Hz, P_b). HRMS (+)ESI m/z found: 678.1312 calc. for $C_{22}H_{30}N_7O_{14}P_2^+$: 678.1320.

Recombinant Tpt1 proteins

Runella slithyformis Tpt1 was produced in *Escherichia coli* and purified as described previously (7). *Candida albicans* and *Candida auris* Tpt1 were produced in *E. coli* and purified as described (25). *Mucor circinelloides* Tpt1 was produced in *E. coli* and purified as described (26). Protein concentrations were determined by using the Biorad dye reagent with bovine serum albumin as the standard.

RNA 2′-phosphotransferase assay

Reaction mixtures (10 µl) containing 100 mM Tris–HCl (pH 7.5), 0.2 µM (2 pmol) 5′ ^{32}P-labeled 6-mer 2′-PO_4 substrate pCpCpAp($A_{2'}$p)pApU (synthesized and radiolabeled as described in (7), 50 µM NAD$^+$ or 2″OMeNAD$^+$ as specified, and Tpt1 as specified in the figure legends were incubated at 37°C. The reactions were quenched at the times specified in the figure legends by addition of three volumes of cold 90% formamide, 50 mM EDTA. The products were analyzed by electrophoresis (at 58 W constant power) through a 40-cm 20% polyacrylamide gel containing 7 M urea in 45 mM Tris-borate, 1 mM EDTA. The radiolabeled 2′-PO_4 RNA substrate pCpCpAp($A_{2'}$p)pApU (migrating fastest), the 2′-OH RNA product pCpCpApApApU, and the RNA 2′-phospho-ADP-ribose intermediate pCpCpAp($A_{2'}$pADPR)pApU (migrating slowest) were well separated (7) and were quantified by scanning the gel with a Typhoon FLA-7000 imaging device and analysis of the gel scan data in ImageQuant TL. Data shown in the graphs are the average of three independent experiments ± SEM.

Results

Synthesis of 2″OMeNAD$^+$ (compound 7)

We explored several approaches to facilitate the synthesis of NAD$^+$ methylated at the 2′-*O* nicotinamide riboside position. Initially, we tried a glycosylation reaction using Koenigs–Knorr conditions, a method previously applied in NAD$^+$ synthesis (27). Starting from 1,3,5-tri-*O*-benzoyl-2-*O*-methyl-α-D-ribofuranose, the resulting product was analysed using mass spectrometry (MS) and 2D-NMR spectroscopy. The major product formed in this reaction was the α-anomer of nicotinamide methoxy-riboside. This stereochemical outcome was observed for both anomers of the starting material, presumably due to the pronounced anomeric effect. In standard nucleoside synthesis, this effect is avoided by neighbouring group participation of the ester protecting group at the 2-hydroxy position. As this cannot be exploited in a glycosylation reaction using a glycosylation donor with a methyl ether at the 2-hydroxy group, a different synthetic approach was investigated.

Zhang *et al.* (28) used trimethylsilyl-trifluoromethanels ulfonate (TMS-Triflate) for glycosylation reactions to successfully receive the β-confirmed 2′-modified NAD$^+$ despite the lack of a directing neighbouring group. To prepare the glycosyl donor (Figure 2A, compound **4**), we opted for a commonly used protection and deprotection cascade, taking advantage of a bridging 3,5-tetraisopropyldisiloxanyl-(TIPDS) protecting group to selective modify the 2-hydroxy group (29). Two different reactions were tested to introduce the 2-*O*-methyl group. Starting from compound **1** (synthesized as described by the Wengel group; (29)), ether synthesis with iodomethane and silver(I)oxide proceeded with high selectivity towards the desired 2-*O*-methylated product (compound **2**). The disadvantage of diminished conversions at lower temperature due to the low boiling point of iodomethane was overcome by using a microwave reactor (40% yield) or by using dimethylformamide (DMF) as solvent and heating (84% yield). The remaining protecting groups were then replaced with acetyl groups to achieve the required glycosylation properties, as the silyl ethers are not stable under the glycosylation reaction conditions, yielding 3,5-diacetoxy-

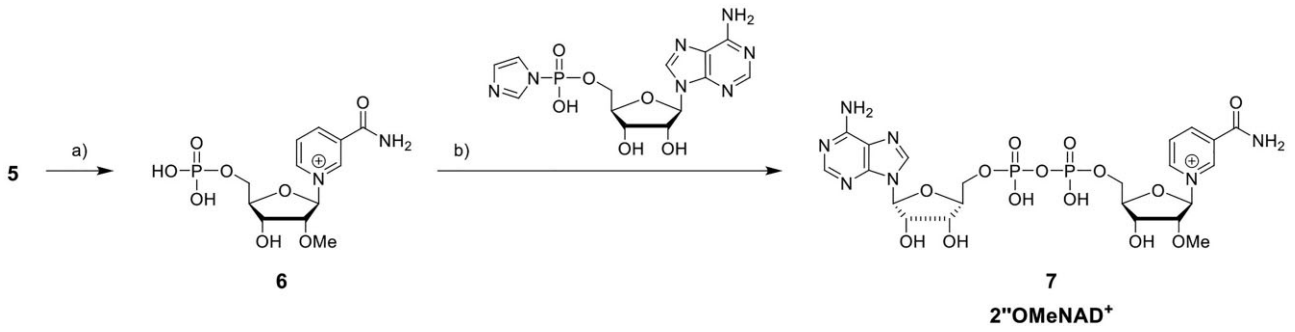

Figure 3. Synthesis of 2″OMeNAD+ (compound **7**). (**A**) $POCl_3$, trimethylphosphate, 0°C, 4 h, 50 %; (**B**) AMP *P*-imidazolide, $MgCl_2$, formamide, r.t., 24 h, 48%.

1,2-dimethoxy-β-D-ribofuranose (Figure 2A, compound 3). The protecting group at the anomeric position was exchanged to an acetyl group by reaction with acetic acid and catalytic amounts of sulfuric acid, resulting in the formation of 1,3,5-triacetoxy-2-methoxy-β-D-ribofuranose (compound **4**). To perform the glycosylation reaction, the prepared glycosyl donor (compound **4**) and the glycosyl acceptor nicotinamide were dissolved in acetonitrile (MeCN) and TMS-triflate was added dropwise according to a published protocol for other modified NAD+ analogues (30). Upon complete conversion of the riboside (compound **4**), we aimed to convert the crude product directly to the deprotected nicotinamide riboside (Figure 2A, compound **5**) by treatment with ammonia in methanol. After HPLC purification, a compound eluted with a retention time of 25 min, and mass spectrometry analysis revealed the expected mass of the desired product. However, a thorough analysis of the HMBC (heteronuclear multiple bond correlation) NMR spectrum (Figure 2B) revealed that the glycosidic bond was formed between the 1-position of the riboside and the amide of the glycosylation donor (Figure 2A, compound **5-R**, a regioisomer of the desired product). To avoid this unwanted reaction, an *in situ* protection of the amide with TMS-triflate was applied by stirring nicotinamide and TMS-triflate in acetonitrile for 30 min prior to the addition of the glycosyl donor (compound **4**). Implementing this method for the synthesis of the nicotinamide riboside, HPLC purification yielded a compound eluting with a decreased retention time (10 min), indicating the formation of the more polar compound **5**, which was verified by NMR analysis (Figure 2C). A prominent HMBC cross signal between the 1′-carbon and the aromatic protons of the nicotinamide suggested the formation of the glycosidic bond with the cyclic nitrogen of the nicotinamide. Furthermore, NOE correlations of the nicotinamide protons with the 3′-proton confirmed the formation of the desired β-conformation of the nicotinamide 2′-methoxyriboside (Figure 2A, compound **5**).

Subsequent phosphorylation with $POCl_3$ at the 5′-hydroxy group yielded the monophosphorylated nicotinamide 2′-methoxyriboside (Figure 3, compound **6**), which was then coupled to AMP *P*-imidazolide, resulting in the formation of 1-(2′-methoxy-β-D-ribofuranosyl)nicotinamide adenine dinucleotide (Figure 3, compound **7**, hereafter referred to as 2″OMeNAD+). This compound was subjected to further biochemical assays to investigate its inhibitory properties against various Tpt1 enzymes.

Utilization of 2″OMeNAD+ by *Runella* Tpt1 blocks step 2 transesterification

We assayed RNA 2′-phosphotransferase activity against 0.2 μM (2 pmol) of a 5′ ^{32}P-labeled 6-mer 2′-PO_4 substrate pCpCpAp(A_2·p)pApU (prepared as described in (7)) as a function of increasing amount of input RslTpt1. After a 30 min incubation at 37°C, the reaction products were resolved by urea-PAGE, which separates the 2′-PO_4 RNA substrate, the 2′-OH RNA product, and the 2′-phospho-ADP-ribosylated RNA intermediate (7). The specific activity of RslTpt1 in the presence of 50 μM NAD+ (Figure 4A, left panel), calculated by linear regression in Prism, was 96.4 ± 1.1 fmol 2′-OH product formed per fmol of Tpt1. No 2′-P-ADPR intermediate was detected in reactions containing 50 μM NAD+. In the absence of added NAD+ (Figure 4A, right panel), we detected a low extent of 2′-OH product formation at super-stoichiometric concentrations of enzyme, which derives from a minority fraction of the RslTpt1 preparation that retains NAD+ (present in *E. coli* at ∼3 mM concentration) during the Tpt1 purification procedure. From the slope of the –NAD+ titration curve, we estimate that 3–4% of the RslTpt1 copurified with NAD+. The salient finding is that the reaction with 50 μM 2″OMeNAD+ resulted in formation of the otherwise undetectable 2′-phospho-ADP-ribosylated RNA, which in this case is an RNA-2′-phospho-(ADP-2″OMe-ribose) dead-end product of step 1 of the Tpt1 pathway (Figure 4A, right panel). This dead-end product accumulated steadily in proportion to stoichiometric levels of input RslTpt1 and comprised 88% of the total labeled RNA at saturating enzyme. The specific activity of RslTpt1 in the presence of 2″OMeNAD+ (Figure 4A, right panel), calculated by linear regression in Prism, was 0.95 ± 1.1 pmol 2′-P-ADPR RNA formed per pmol of Tpt1. We hypothesize that the RNA-2′-phospho-(ADP-2″OMe-ribose) occupies both the RNA lobe and the NAD+ lobe and, being chemically unreactive in step 2 transesterification, remains trapped *in situ* on the Tpt1 enzyme. In the presence of 2″OMeNAD+, the extent of 2′-OH product formation by the minor fraction of NAD+-bound RslTpt1 was similar to that observed in the absence of added NAD+ (Figure 4A, right panel).

The kinetic profile of the reaction of 0.5 μM RslTpt1 with 0.2 μM 2′-PO_4 RNA substrate and 50 μM 2″OMeNAD+ is shown in Figure 4B. The reaction achieved an endpoint at which 93% of the 2′-PO_4 RNA substrate was converted to RNA-2′-phospho-(ADP-2″OMe-ribose). The apparent rate constant for this reaction was 0.58 ± 0.023 min^{-1}. In a previous study, we had found that reaction of RslTpt1

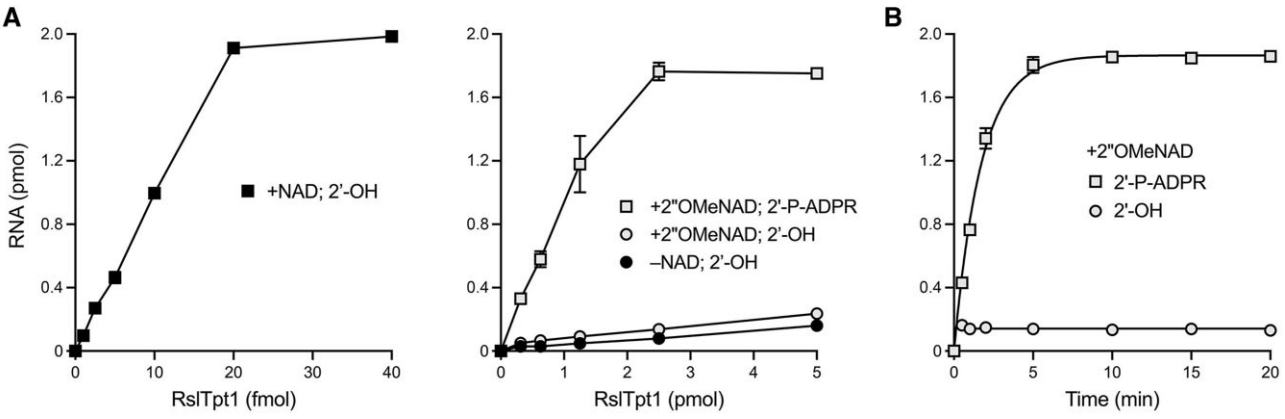

Figure 4. Utilization of 2″OMeNAD$^+$ by *Runella* Tpt1 generates a dead-end 2′-phospho-ADP-ribosylated RNA. (**A**) Tpt1 titrations. Reaction mixtures (10 μl) containing 100 mM Tris–HCl (pH 7.5), 0.2 μM (2 pmol) 5′ ^{32}P-labeled 6-mer 2′-PO$_4$ substrate, either 50 μM NAD$^+$ (left panel), no added NAD$^+$ (middle panel), or 50 μM 2″OMeNAD$^+$ (middle panel), and RslTpt1 as specified on the x-axes were incubated at 37°C for 30 min. The extents of formation of 2′-OH end-product and abortive 2′-P-ADPR intermediate are plotted as a function of input Tpt1. Each datum in the graphs is the average of three independent titration experiments ± SEM. (**B**) Kinetics of the reaction with 2″OMeNAD$^+$. Reaction mixtures (100 μl) containing 100 mM Tris–HCl (pH 7.5), 0.2 μM 5′ ^{32}P-labeled 6-mer 2′-PO$_4$ substrate, 50 μM 2″OMeNAD$^+$, and 0.5 μM RslTpt1 were incubated at 37°C. The reactions were initiated by adding RslTpt1 to a pre-warmed reaction mixture. Aliquots (10 μl, containing 2 pmol of 2′-PO$_4$ RNA substrate) were withdrawn at the times specified on the x-axis and quenched immediately with cold formamide/EDTA. The extents of formation of 2′-P-ADPR RNA and 2′-OH RNA are plotted as a function of reaction time. Each datum in the graphs is the average of three independent time course experiments ± SEM. The data were fit by nonlinear regression to a one phase association in Prism.

with 50 μM ara-2″F-NAD$^+$ resulted in trapping an RNA-2′-phospho-(ADP-2″-fluoroarabinose) dead-end product of step 1 of the Tpt1 pathway, albeit with ∼8-fold slower kinetics ($k = 0.077$ min^{-1}) (17). Thus, a 2″-substituted ribose analog of NAD$^+$ serves as a better starting point for a Tpt1 poison vis-à-vis a 2″-substituted arabinose analog.

2″OMeNAD$^+$ traps RslTpt1 on the RNA-2′-phospho-(ADP-2″OMe-ribose) dead-end product

We implemented an electrophoretic mobility shift assay (EMSA) to gauge whether the 2′-phospho-2″OMeADP-ribosylated RNA remains stably associated with RslTpt1. EMSA analysis of a series of reaction mixtures containing: (i) 2 pmol 5′ ^{32}P-labeled 6-mer 2′-PO$_4$ RNA substrate and no RslTpt1; (ii) 2 pmol 2′-PO$_4$ RNA substrate and 5 pmol RslTpt1 with no NAD$^+$; (iii) 2 pmol 2′-PO$_4$ RNA substrate, 5 pmol RslTpt1 and 50 μM NAD$^+$; and (iv) 2 pmol 2′-PO$_4$ RNA substrate, 5 pmol RslTpt1 and 50 μM 2″OMeNAD$^+$ is shown in Figure 5A. This experiment shows that there was no detectable association of RslTpt1 with the 2′-OH RNA product generated during the reaction that contained NAD$^+$. By contrast, nearly all of the RNA formed during the reaction that contained 2″OMeNAD$^+$ was shifted upward in the gel to form a discrete Tpt1•RNA-2′-phospho-(OMeADPR) complex (Figure 5A). We surmise that the low residual level of free ^{32}P-RNA detected in this reaction corresponds to the 2′-OH RNA product formated by the minor fraction of NAD$^+$-bound RslTpt1 (discussed above). This experiment also highlighted that binary interaction of RslTpt1 with the input 2′-PO$_4$ RNA substrate (i.e. in the absence of NAD$^+$) is unstable, as reflected in the trailing comet of radioactivity immediately above the free RNA (Figure 5A), which we take to indicate that the substrate dissociated from RslTpt1 during the electrophoretic run.

The Rsl1Tpt titration experiment shown in Figure 5B affirms that the extent of formation of the stable Tpt1•RNA-2′-phospho-(OMeADPR) complex during reaction with 2″OMeNAD$^+$ occurs with near 1:1 stoichiometry of substrate and enzyme. Thus, not only does 2″OMeNAD$^+$ poison the Tpt1 reaction after completion of step 1, it sequesters RslTpt1 bound to the dead-end product.

2″OMeNAD$^+$ is not an effective substrate for Tpt1 from three fungal pathogens

To gauge whether 2″OMeNAD$^+$ is an effective dead-end trap for fungal Tpt1 enzymes, we tested the ability of Tpt1 enzymes from three human fungal pathogens—*Candida albicans*, *Candida auris* and *Mucor circinelloides*—to utilize 2″OMeNAD$^+$ in lieu of NAD$^+$. *Candida albicans*, a commensal yeast colonizer of humans, causes a spectrum of illnesses ranging from local infections of oral, esophageal, and genital mucosa to life-threatening invasive systemic infections in immunocompromised hosts. *Candida auris*, first isolated in 2009 in Japan, has since emerged globally as a multi-drug-resistant invasive fungal pathogen that poses a dire health threat in hospitalized patient populations. Mucormycosis is a serious, often fatal, infection acquired either by inhalation of fungal spores leading to infection of the sinuses, brain, and/or lungs or by entry of spores through a break in the skin following a burn or other skin trauma. Risk factors for mucormycosis include diabetes, steroid use, cancer, organ transplant, and COVID-19 infection. The aforementioned fungi are among the pathogens designated by the World Health Organization as priorities for research and public health action (30).

In the experiment shown in Figure 6, the three fungal Tpt1 enzymes were assayed in parallel with RslTpt1, which provided a positive control for effective trapping of the dead-end intermediate by 2″OMeNAD$^+$. Each of the fungal enzymes quantitatively removed the RNA 2′-PO$_4$ in the presence of 50 μM NAD$^+$ (Figure 6). The instructive (and disappointing) findings were that 2″OMeNAD$^+$ failed to support effective catalysis of step 1 of the Tpt1 pathway by any of the fungal pathogen enzymes. To wit, only 3.9% of the 2′-PO$_4$ substrate was converted to 2-P-ADPR by *C. albicans* Tpt1, while

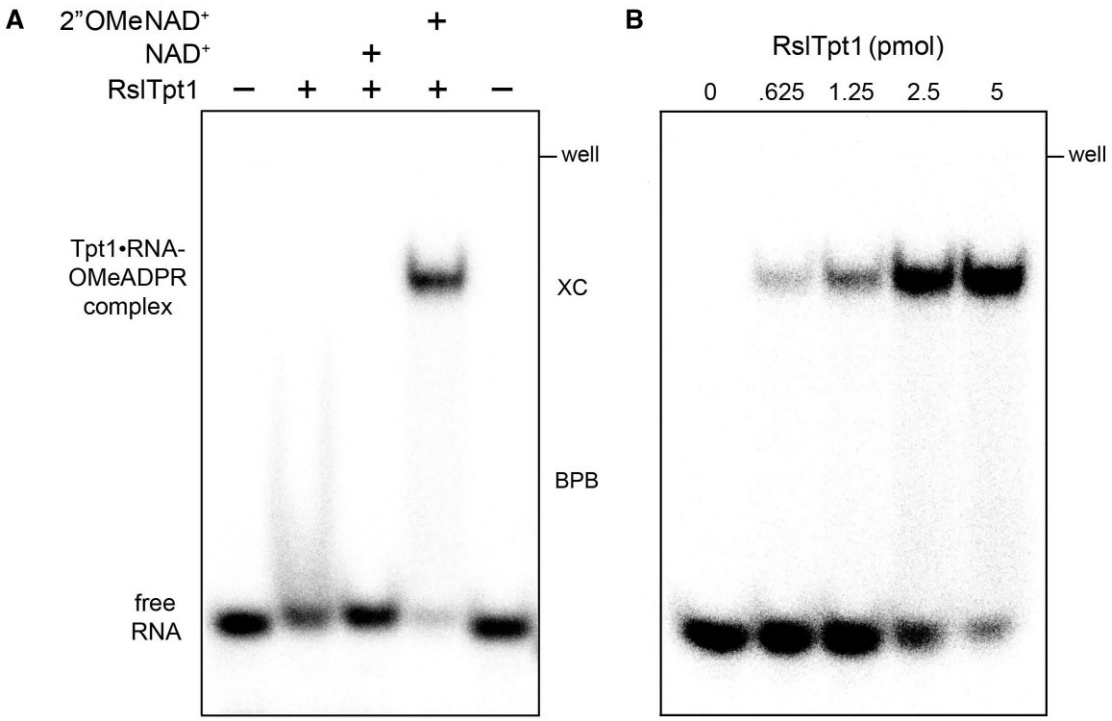

Figure 5. 2″OMeNAD$^+$ traps Tpt1 on the RNA-2′-phospho-(ADP-2″OMe-ribose) dead-end product. (**A**) Reaction mixtures (10 μl) containing 100 mM Tris–HCl (pH 7.5), 0.2 μM (2 pmol) 5′ ^{32}P-labeled 6-mer 2′-PO_4 substrate, either no added NAD$^+$, 50 μM NAD$^+$, or 50 μM 2″OMeNAD$^+$, and 5 pmol RslTpt1 (where indicated by + above the lanes) were incubated at 37°C for 15 min. The mixtures were adjusted to 5% (v/v) glycerol and then applied to a 15-cm native 8% polyacrylamide gel containing 0.25x TBE that had been pre-run at 110 V for 30 min. Separation of RslTpt1-bound and free RNA was achieved by electrophoresis for 2.5 h at 110 V at room temperature. The radiolabeled species were visualized by scanning the gel with a Typhoon FLA-7000 imaging device. The positions of the sample well and xylene cyanol (XC) and bromophenol blue (BPB) dye makers run in a parallel lane are indicated on the right. (**B**) Reaction mixtures (10 μl) containing 100 mM Tris–HCl (pH 7.5), 0.2 μM (2 pmol) 5′ ^{32}P-labeled 6-mer 2′-PO_4 substrate, 50 μM 2″OMeNAD$^+$ and RslTpt1 as specified above the lanes were incubated at 37°C for 15 min, adjusted to 5% glycerol, and then analyzed by native PAGE.

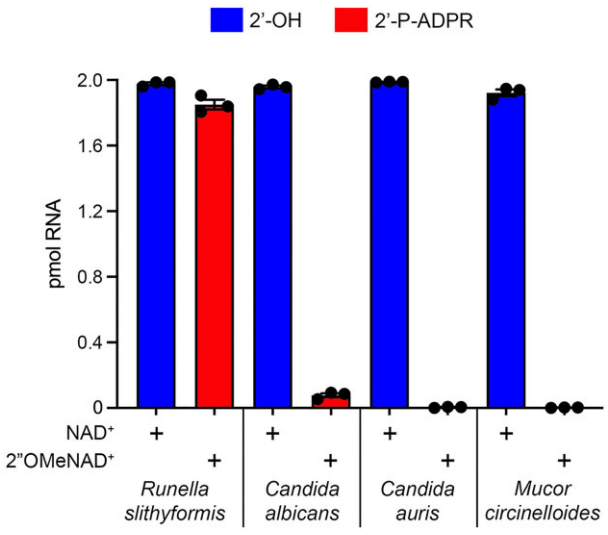

Figure 6. 2″OMeNAD$^+$ is not an effective substrate for Tpt1 from three fungal pathogens. Reaction mixtures (10 μl) containing 100 mM Tris–HCl (pH 7.5), 0.2 μM (2 pmol) 5′ ^{32}P-labeled 6-mer 2′-PO_4 substrate, either 50 μM NAD$^+$ or 50 μM 2″OMeNAD$^+$ (where indicated by +), and 0.5 μM (5 pmol) Tpt1 from the species specified on the x-axis were incubated at 37°C for 30 min. The extents of formation of 2′-OH RNAs in reactions containing NAD$^+$ (blue bars) and formation of RNA-2′-phospho-(ADP-2″OMe-ribose) in reactions containing 2″OMeNAD$^+$ (red bars) are shown. Data are the average of three independent experiments ± SEM.

C. auris Tpt1 (0.2%. conversion) and *Mucor* Tpt1 (0.1% conversion) were virtually inert.

Discussion

Interest in the chemical biology of Tpt1 is prompted by its candidacy as a target for discovery of anti-fungal drugs, based on the facts that: (i) Tpt1 is essential for viability in the model fungi *Saccharomyces cerevisiae* and *Schizosaccharomyces pombe* and in the pathogenic fungus *Candida albicans* (4,31,32) and is virtually certain to be essential in other human fungal pathogens and (ii) the chemical/enzymatic mechanism of tRNA splicing in metazoa—mediated by the RNA ligase RtcB—is entirely different from that of fungi and does not result in a junction 2′-PO_4 (33).

One can conceive of two ways to interdict Tpt1 activity: (i) by inhibiting transfer of ADP-ribose from NAD$^+$ to 2′-PO_4 RNA, thereby resulting in the accumulation of spliced tRNAs that retain the 2′-PO_4 in the anticodon loop or (ii) by inhibiting the transesterification step and trapping the ADP-ribosylated RNA intermediate, thereby generating tRNAs with bulky lesions in the anticodon loop. The former is a classic inhibitor scenario which can be overcome by producing more of the Tpt1 enzyme. The latter is a 'poison' scheme in which production of more Tpt1 would only exacerbate the accumulation of dead-end product complexes. It is worth noting that DNA topoisomerase poisons that trap covalent Topo–DNA intermediates are among the most successful and widely used anti-bacterial and anti-cancer agents in clinical practice.

The substrate analog 2″OMeNAD$^+$ (compound 7), chemically synthesized via a novel protocol, is shown in this study to trap an abortive ADP-ribosylated RNA intermediate synthesized by RslTpt1 and to sequester the enzyme bound to the dead-end product. Our results have implications (positive and negative), for the development of Tpt1 poisons as anti-fungals and efforts to capture structures of Tpt1 enzymes as a step 1 product complex and/or step 2 Michaelis complex.

The encouraging success in poisoning RslTpt1 with 2″OMeNAD$^+$ is countered by the failure of 2″OMeNAD$^+$ to serve as a substrate for Tpt1 enzymes from three different human fungal pathogens. [The finding that Tpt1s from different taxa vary in their ability to utilize 2″OMeNAD$^+$ in lieu of NAD$^+$ echoes previous experience with ara-2″F NAD$^+$, which is utilized as an effective substrate for step 1 by RslTpt1 but not by Tpt1s from *Aspergillus*, *Coccidioides*, and *Candida* species (17,25).] We envision that the 2″OMe group of 2″OMeNAD$^+$ introduces detrimental steric clash in the active site of some Tpt1s (e.g. the fungal enzymes) but apparently not in RslTpt1.

Solution NMR studies of RslTpt1 highlighted how the separately well-folded N-terminal RNA lobe and C-terminal NAD$^+$ lobe modules are arrayed in solution with a high degree of positional freedom with respect to one another and that NAD$^+$ binding to the C-lobe does not suffice to impose order on the system (16). This domain mobility resonates with, and likely accounts for, our inability to grow crystals of RslTpt1, in unliganded form or in the presence of NAD$^+$. The freedom of movement of the RslTpt1 lobes in solution owes to the conformational flexibility of the inter-domain linker (16). The linker segment varies in length among Tpt1 orthologs and its primary structure is not well conserved. We suspect that the flexibility and/or plasticity of RslTpt1 allows it to accept 2″OMeNAD$^+$ as a step 1 substrate. In this vein, a reaction of 2″OMeNAD$^+$ with 2′-PO_4 RNA should enable the otherwise dynamic RslTpt1 lobes to be 'locked down' in a step 1 product complex and thus more amenable to crystallization and structure determination.

Insights gained from the present study of 2″OMeNAD$^+$ point us toward alternative 2″-substituted NAD$^+$ analogs (e.g. 2″-F, 2″-Cl, 2″-NH_2) as candidate fungal Tpt1 poisons. 2″-fluoroNAD$^+$ would appear to be a most promising NAD$^+$ isostere that might evade steric clash and poison the fungal enzymes. A chemi-enzymatic synthesis of 2″-fluoroNAD$^+$ has been reported (34). We are pursuing alternative strategies for fully chemical synthesis of 2″-fluoroNAD$^+$.

Finally, the ability to chemically synthesize 2″OMeNAD$^+$ provides a useful analog for mechanistic studies of other NAD$^+$-dependent ADP-ribosyltransferases. For example: (i) utilization of 2″OMeNAD$^+$ by sirtuins could lead to trapping of the alkylimidate intermediate; and (ii) utilization of 2″OMeNAD$^+$ by poly-ADP-ribose (PAR) polymerases (PARP enzymes) could interdict generation of 2″-*O*-branched PAR chains.

Data availability

The data underlying this article are available in the article and in its online supplementary information.

Supplementary data

Supplementary Data are available at NAR Online.

Funding

U.S. National Institutes of Health [R35-GM126945 to S.S.]; Deutsche Forschungsgemeinschaft [MA 2288/21-1 to A.M.]; Alexander von Humboldt Foundation (to R.K.). Funding for open access charge: National Institutes of Health [R35-GM126945].

Conflict of interest statement

None declared.

References

1. Suskiewicz,M.J., Prokhorova,E., Rack,J.G. and Ahel,I. (2023) ADP-ribosylation from molecular mechanisms to therapeutic implications. *Cell*, **186**, 4475–4495.
2. Sauve,A.A. and Youn,D.Y. (2012) Sirtuins: NAD$^+$-dependent deacetylase mechanism and regulation. *Curr. Opin. Chem. Biol.*, **16**, 535–543.
3. Bursch,K.L., Goetz,C.J. and Smith,B.C. (2024) Current trends in sirtuin activator and inhibitor development. *Molecules*, **29**, 1185.
4. Culver,G.M., McCraith,S.M., Consaul,S.A., Stanford,D.R. and Phizicky,E.M. (1997) A 2′-phosphotransferase implicated in tRNA splicing is essential in *Saccharomyces cerevisiae*. *J. Biol. Chem.*, **272**, 13203–13210.
5. Spinelli,S.L., Malik,H.S., Consaul,S.A. and Phizicky,E.M. (1998) A functional homolog of a yeast tRNA splicing enzyme is conserved in higher eukaryotes and in *Escherichia coli*. *Proc. Natl. Acad. Sci. U.S.A.*, **95**, 14136–14141.
6. Sawaya,R., Schwer,B. and Shuman,S. (2005) Structure-function analysis of the yeast NAD$^+$-dependent tRNA 2′-phosphotransferase Tpt1. *RNA*, **11**, 107–113.
7. Munir,A., Abdullahu,L., Damha,M.J. and Shuman,S. (2018) Two-step mechanism and step-arrest mutants of *Runella slithyformis* NAD$^+$-dependent tRNA 2′-phosphotransferase Tpt1. *RNA*, **24**, 1144–1157.
8. Munir,A., Banerjee,A. and Shuman,S. (2018) NAD$^+$-dependent synthesis of a 5′-phospho-ADP-ribosylated RNA/DNA cap by RNA 2′-phosphotransferase Tpt1. *Nucleic Acids Res.*, **46**, 9617–9624.
9. Ohira,T., Monowa,K., Sugiyama,K., Yamashita,S., Sakaguchi,Y., Miyauchi,K., Noguchi,R., Kaneko,A., Orita,I., Fukui,T., *et al.* (2022) Reversible RNA phosphorylation stabilizes tRNA for cellular thermotolerance. *Nature*, **605**, 372–379.
10. Harding,H.P., Lackey,J.G., Hsu,H.C., Zhang,Y., Deng,J., Xu,R.M., Damha,M.J. and Ron,D. (2008) An intact unfolded protein response in Trpt1 knockout mice reveals phylogenic divergence in pathways for RNA ligation. *RNA*, **14**, 225–232.
11. McCraith,S.M. and Phizicky,E.M. (1991) An enzyme from *Saccharomyces cerevisiae* uses NAD$^+$ to transfer the splice junction 2′-phosphate from ligated tRNA to an acceptor molecule. *J. Biol. Chem.*, **266**, 11986–11992.
12. Culver,G.M., McCraith,S.M., Zillman,M., Kierzek,R., Michaud,N., LaReau,R.D., Turner,D.H. and Phizicky,E.M. (1993) An NAD derivative produced during transfer RNA splicing: aDP-ribose 1"-2" cyclic phosphate. *Science*, **261**, 206–208.
13. Spinelli,S.L., Kierzek,R., Turner,D.H. and Phizicky,E.M. (1999) Transient ADP-ribosylation of a 2′-phosphate implicated in its removal from ligated tRNA during splicing in yeast. *J. Biol. Chem.*, **274**, 2637–2644.
14. Steiger,M.A., Jackman,J.E. and Phizicky,E.M. (2005) Analysis of 2′-phosphotransferase (Tpt1p) from *Saccharomyces cerevisiae*: evidence for a conserved two-step reaction mechanism. *RNA*, **11**, 99–106.
15. Banerjee,A., Munir,A., Abdullahu,L., Damha,M.J., Goldgur,Y. and Shuman,S. (2019) Structure of tRNA splicing enzyme Tpt1

illuminates the mechanism of RNA 2′-PO_4 recognition and ADP-ribosylation. *Nature Comm*., **10**, 218.
16. Alphonse,S., Banerjee,A., Dantuluri,S., Shuman,S. and Ghose,R. (2021) NMR solution structures of *Runella slithyformis* RNA 2′-phosphotransferase Tpt1 provide insights into NAD^+ binding and specificity. *Nucleic Acids Res*., **49**, 9607–9624.
17. Dantuluri,S., Abdullahu,L., Munir,A., Katolik,A., Damha,M.J. and Shuman,S. (2020) Substrate analogs that trap the 2′-phospho-ADP-ribosylated RNA intermediate of the Tpt1 (tRNA 2′-phosphotransferase) reaction pathway. *RNA*, **26**, 373–381.
18. Jacewicz,A., Dantuluri,S. and Shuman,S. (2023) Structural basis for Tpt1-catalyzed 2′-PO_4 transfer from RNA and NADP(H) to NAD^+. *Proc. Natl. Acad. Sci. U.S.A*., **120**, e2312999120.
19. Slama,J. and Simmons,A.M. (1988) Carbonicotinamide adenine. Dinucleotide: synthesis and enzymological properties of a carbocyclic analogue of oxidized nicotinamide adenine dinucleotide. *Biochemistry*, **27**, 183–193.
20. Szczepankiewicz,B.G., Dai,H., Koppetsch,K.J., Qian,D., Jiang,F., Mao,C. and Perni,R.B. (2012) Synthesis of carba-NAD and the structures of its ternary complexes with SIRT3 and SIRT5. *J. Org. Chem*., **77**, 7319–7329.
21. Sleath,P.R., Handlon,A.L. and Oppenheimer,N.J. (1991) Pyridine coenzyme analogues. 3. Synthesis of three NAD^+ analogues containing a 2′-deoxy-2′-substituted nicotinamide arabinofuranosyl moiety. *J. Org. Chem*., **56**, 3608–3613.
22. Muller-Steffner,H.M., Malver,O., Hosie,L., Oppenheimer,N.J. and Schuber,F. (1992) Slow-binding inhibition of NAD^+ glycohydrolase by arabino analogues of β-NAD^+. *J. Biol. Chem*., **267**, 9606–9611.
23. Egea,P.F., Muller-Steffner,H., Kuhn,I., Cakir-Kiefer,C., Oppenheimer,N.J., Stroud,R.M., Kellenberger,E. and Schuber,F. (2012) Insights into the mechanism of bovine CD38/NAD^+ glycohydrolase from the X-ray structures of its Michaelis complex and covalently-trapped intermediates. *PLoS One*, **7**, e34918.
24. Mukaiyama,T. and Hashimoto,M. (2006) Phoshorylation by oxidation-reduction condensation: preparation of active phosphorylating reagents. *Bull. Chem. Soc. Japan*, **44**, 2284.
25. Dantuluri,S., Schwer,B., Abdullahu,L., Damha,M.J. and Shuman,S. (2021) Activity and substrate specificity of *Candida*, *Aspergillus*, and *coccidioides* Tpt1: essential tRNA splicing enzymes and potential anti-fungal targets. *RNA*, **27**, 616–627.
26. Ghosh,S., Dantuluri,S., Jacewicz,A., Sanchez,A.M., Abdullahu,L., Damha,M.J., Schwer,B. and Shuman,S. (2024) Characterization of tRNA splicing enzymes RNA ligase and tRNA 2′-phosphotransferase from the pathogenic fungi Mucorales. *RNA*, **30**, 367–380.
27. Rieth,S., Spliesgar,D., Orth,J., Lehner,M., Kasprzyk,R., Stengel,F. and Marx,A. (2024) A desthiobiotin labelled NAD^+ analogue to uncover poly(ADP-ribose) polymerase 1 protein targets. *ChemBioChem*, **25**, e202300797.
28. Zhang,X.N., Cheng,Q., Chen,J., Lam,A.T., Lu,Y., Dai,Z., Pei,H., Evdokimov,N.M., Louie,S.G. and Zhang,Y. (2019) A ribose-functionalized NAD^+ with unexpected high activity and selectivity for protein poly-ADP-ribosylation. *Nature Comm*., **10**, 4196.
29. Gotfredsen,C.H., Jacobsen,J.P. and Wengel,J. (1996) Synthesis and properties of α- and β-oligodeoxynucleotides containing α- and β-1-(2-O-methyl-d-arabinofuranosyl)thymine. *Bioorg. Med. Chem*., **4**, 1217–1225.
30. World Health Organization (2022) In: *WHO Fungal Priority Pathogens List to Guide Research, Development, and Public Health Action*. License: CC BY-NC-SA 3.0 IGO.
31. Kim,D.U., Hayles,J., Kim,D., Wood,V., Park,H.O., Won,M., Yoo,H.S., Duhig,T., Nam,M., Palmer,G., *et al.* (2010) Analysis of a genome-wide set of gene deletions in the fission yeast *Schizosaccharomyces pombe*. *Nat. Biotechnol*., **28**, 617–623.
32. Segal,E.S., Gritsenko,V., Levitan,A., Yadav,B., Dror,N., Steenwyk,J.L., Silberberg,Y., Meilich,K., Rokas,A., Gow,N.A., *et al.* (2018) Gene essentiality analyzed by in vivo transposon mutagenesis and machine learning in a stable haploid isolate of *Candida albicans*. *mBio*, **9**, e02048-18.
33. Shuman,S. (2023) RNA repair: hiding in plain sight. *Annu. Rev. Genet*., **57**, 461–489.
34. Cen,Y. and Sauve,A.A. (2009) Diastereocontrolled electrophilic fluorinations of 2-deoxyribonolactone: syntheses of all corresponding 2′-deoxy-2′-fluorolactones and 2-deoxy-2-fluoro-NAD^+s. *J. Org. Chem*., **74**, 5779–5789.

Received: June 17, 2024. **Revised:** July 24, 2024. **Editorial Decision:** July 25, 2024. **Accepted:** July 31, 2024